

01 Jan 2015

Electrical Resistivity Imaging for Long-Term Autonomous Monitoring of Hydrocarbon Degradation: Lessons from the Deepwater Horizon Oil Spill

Jeffrey W. Heenan

Lee D. Slater

Dimitrios Ntarlagiannis

Estella A. Atekwana

Missouri University of Science and Technology, atekwana@mst.edu

et. al. For a complete list of authors, see https://scholarsmine.mst.edu/geosci_geo_peteng_facwork/1292

Follow this and additional works at: https://scholarsmine.mst.edu/geosci_geo_peteng_facwork



Part of the [Geology Commons](#)

Recommended Citation

J. W. Heenan et al., "Electrical Resistivity Imaging for Long-Term Autonomous Monitoring of Hydrocarbon Degradation: Lessons from the Deepwater Horizon Oil Spill," *Geophysics*, vol. 80, no. 1, pp. B1-B11, Society of Exploration Geophysicists, Jan 2015.

The definitive version is available at <https://doi.org/10.1190/geo2013-0468.1>

This Article - Journal is brought to you for free and open access by Scholars' Mine. It has been accepted for inclusion in Geosciences and Geological and Petroleum Engineering Faculty Research & Creative Works by an authorized administrator of Scholars' Mine. This work is protected by U. S. Copyright Law. Unauthorized use including reproduction for redistribution requires the permission of the copyright holder. For more information, please contact scholarsmine@mst.edu.

Electrical resistivity imaging for long-term autonomous monitoring of hydrocarbon degradation: Lessons from the Deepwater Horizon oil spill

Jeffrey Heenan¹, Lee D. Slater¹, Dimitrios Ntarlagiannis¹, Estella A. Atekwana²,
Babu Z. Fathepure³, Sonal Dalvi³, Cameron Ross²,
Dale D. Werkema⁴, and Eliot A. Atekwana²

ABSTRACT

Conceptual models for the geophysical responses associated with hydrocarbon degradation suggest that the long-term evolution of an oil plume will result in a more conductive anomaly than the initial contamination. In response to the Deepwater Horizon (DH) oil spill into the Gulf of Mexico in 2010, an autonomous resistivity monitoring system was deployed on Grand Terre, Louisiana, in an attempt to monitor natural degradation processes in hydrocarbon-impacted beach sediments of this island. A 48-electrode surface array with a 0.5-m spacing was installed to obtain twice-daily images of the resistivity structure of the shallow subsurface impacted by oil. Over the

course of approximately 18 months, we observed a progressive decrease in the resistivity of the DH spill-impacted region. Detailed analysis of pixel/point resistivity variation within the imaged area showed that long-term decreases in resistivity were largely associated with the DH-impacted sediments. A microbial diversity survey revealed the presence of hydrocarbon-degrading organisms throughout the test site. However, hydrocarbon degradation activity was much higher in the DH-impacted locations compared to nonimpacted locations, suggesting the presence of active hydrocarbon degraders, supporting biodegradation processes. The results of this long-term monitoring experiment suggested that resistivity might be used to noninvasively monitor the long-term degradation of crude oil spills.

INTRODUCTION

The present trend toward more sustainable remediation (Ellis, 2009), and, in turn, the need for more robust tools for long-term monitoring, demands innovative applications of established and new techniques, including geophysical methods. Advances in technology and improved understanding of geophysical signals have allowed for geophysical methods such as electric resistivity to be used for mapping, monitoring, and characterization of contaminants. Advantages such as cost efficiency, non- or minimally invasive application, high temporal and spatial resolution, and the

recently shown potential for autonomous operation (LaBrecque et al., 2004; Versteeg et al., 2006; Johnson et al., 2012; Robinson et al., 2012) make electrical geophysical methods a viable option for long term monitoring projects.

Geophysical methods are increasingly being used for detection/monitoring of microbial processes within earth media (Atekwana et al., 2006; Atekwana and Slater, 2009). The presence and activity of microorganisms have been documented to impact geophysical signals, such as electric resistivity (Atekwana et al., 2000). Alterations in pore-fluid chemistry, the formation/removal of solid phases, and the addition of biodegradation by-products have been

Manuscript received by the Editor 16 December 2013; revised manuscript received 16 September 2014; published online 22 December 2014.

¹Rutgers University, Department of Earth and Environmental Sciences, Newark, New Jersey, USA. E-mail: jheenan@pegasus.rutgers.edu; dimntar@rutgers.edu; lslater@rutgers.edu.

²Oklahoma State University, Boone Pickens School of Geology, Stillwater, Oklahoma, USA. E-mail: estella.atekwana@okstate.edu; camersr@ostatemail.okstate.edu; eliot.atekwana@okstate.edu.

³Oklahoma State University, Microbiology and Molecular Genetics, Stillwater, Oklahoma, USA. E-mail: babu.fathepure@okstate.edu; sonal.dalvi@okstate.edu.

⁴United States Environmental Protection Agency, Las Vegas, Nevada, USA. E-mail: werkema.d@epamail.epa.gov.

© 2014 Society of Exploration Geophysicists. All rights reserved.

documented to change geophysical signatures over mature hydrocarbon-contaminated sites (Atekwana and Atekwana, 2010). These observations have led to the development of a model explaining changes in resistivity related to the long-term degradation of hydrocarbon (Figure 1a). Contrary to the traditional expectation of electrically insulating hydrocarbon plumes, this conceptual model suggests that, in aged hydrocarbon-impacted zones, the resistivity of the contaminated area is lower relative to the resistivity of the bulk formation (Atekwana et al., 2000; Sauck, 2000; Bradford,

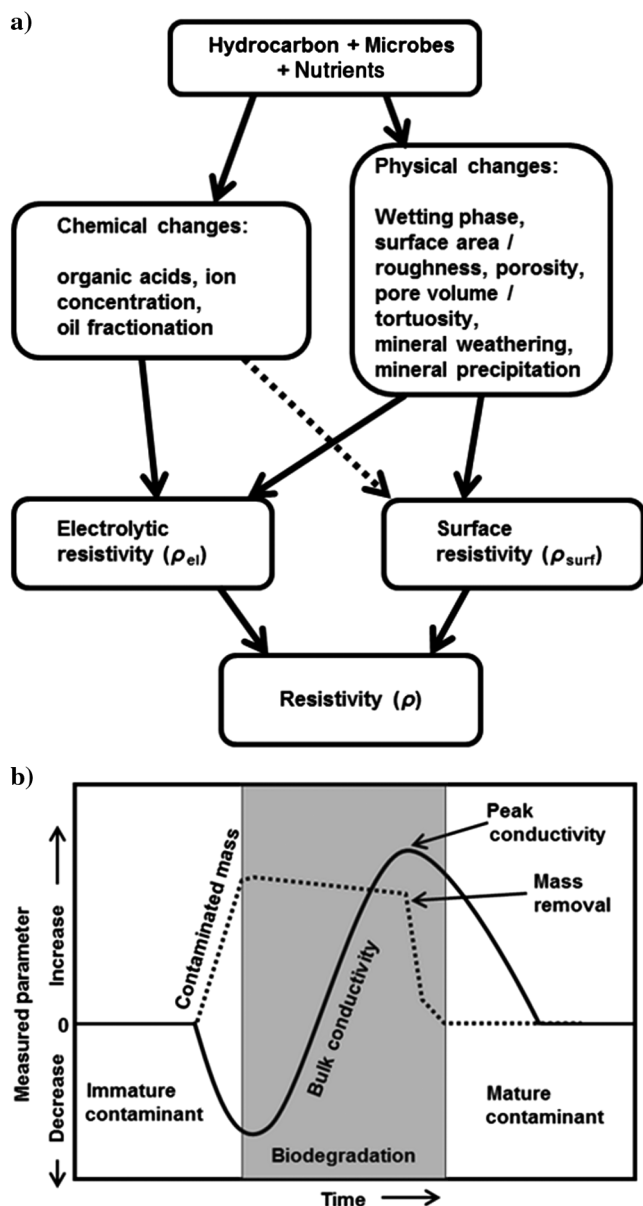


Figure 1. (a) Conceptual model of the factors that influence resistivity in an area of active hydrocarbon degradation. (b) Conceptual diagram showing the initial contamination resulting in a decrease in conductivity and an increase in contaminated mass. As biodegradation progresses to completion, the bulk conductivity increases with the concentration of the biodegradation by-products as the contaminated mass decreases. The system returns to its initial state upon the completion of biodegradation.

2007; Cassidy, 2007, 2008; Atekwana and Slater, 2009; Atekwana and Atekwana, 2010). This model also suggests that young, resistive hydrocarbon spills become more conductive as (bio)degradation proceeds and the spill ages. Increases in dissolved solids, due to the microbial induced mineral weathering, and oil emulsification, due to biosurfactant production, are among the explanations for the observed decrease in resistivity over time (Sauck et al., 1998; Atekwana et al., 2000). The expected evolution of electric conductivity is visualized conceptually in Figure 1b in which the initial contamination causes an increase in organic contaminated mass and a corresponding decrease in conductivity. As biodegradation progresses to completion, decreases in contaminant mass and associated increases in the concentration of biodegradation by-products (i.e., increased ionic concentration) decrease the bulk conductivity. Upon completion of biodegradation, the system largely returns to its initial conductivity state.

Here, we report on long-term electrical resistivity imaging (ERI) associated with natural biodegradation of a young hydrocarbon spill resulting from the BP Deepwater Horizon (DH) disaster in 2010. This experiment was designed to monitor a relatively fresh spill from its early stages to maturity; to our knowledge, this is the first study to document the evolution in electric resistivity of such an immature contamination in a saline marine environment.

Study site

On 20 April 2010, oil and gas escaped from BP's DH exploratory Macondo well located 130 miles to the southeast of the southern tip of the Mississippi Delta (Operational Science Advisory Team, 2011). The DH oil spill resulted in the release of approximately 4.4 million barrels of crude oil into the Gulf of Mexico and surrounding areas (Crone and Tolstoy, 2010); 2.1 million gallons of dispersants were applied at the ocean surface and wellhead in an effort to contain/fight the spill (Operational Science Advisory Team, 2011). This massive oil spill impacted a large portion of the gulf coastline, including beaches, marshes, and wetlands. Although an ecological catastrophe, the DH oil spill provided a unique opportunity for scientists to study a spill from its inception, determine the impact on marine/plant/animal life, and monitor natural degradation processes.

Preliminary data on the oil spill (Geospatial Platform Resource Center, 2013) suggested heavy impact on the beaches/marshes of southern Louisiana (LA), approximately 180-miles northwest of the accident site, including the Grand Terre (GT1) barrier islands off the southeastern coast of LA (Figure 2). The first physical evidence of crude oil contamination was observed in early July 2010, in the form of tar balls washing up on the shores of Grand Isle, LA (Operational Science Advisory Team, 2011). Remediation efforts led by BP on the shores of Grand Isle and GT1 consisted of spatial delineation of the crude oil by auguring holes and marking if any crude oil was visible in the soil. Oil delineation was followed by separating the visually contaminated sediment from the uncontaminated sediment, either by shovel or by mechanical sifting equipment and shipping it off site for treatment.

Our study site, located on GT1, was well suited for uninterrupted long-term monitoring because it is uninhabited, was severely impacted by the oil spill, remediation efforts excluded heavy equipment due to its nature reserve status, and certain areas were left untreated to allow natural remediation to take its course. The experimental plot, located on the northeast tip of GT1 (Figure 2) in which

no remediation efforts took place, was centered on an area with an identified subsurface oil layer approximately 15-cm thick and at approximately 60-cm below the surface, based on observations from test pits, at the time of the monitoring system deployment.

MATERIALS AND METHODS

Electrical resistivity imaging

ERI is used to calculate the resistivity (ρ) distribution within the subsurface by injecting current and measuring the resulting potential differences on a dense array of electrodes (Binley and Kemna, 2005). This method has been extensively applied for monitoring saline intrusions (Slater et al., 2000), moisture transport in the vadose zone (Daily et al., 1992; Binley et al., 2002), and leaks from storage tanks (Daily et al., 2004; Rucker et al., 2011). The conventional regularization approach in ERI is to solve for the model with minimal structure that fits the data to some prescribed level of tolerance that is determined by the measurement errors (deGroot-Hedlin and Constable, 1990). In this experiment, the following objective function was minimized:

$$\phi(m) = \|W_d[d - f(m)]^2\| + \alpha \|W_m[m - m_{\text{ref}}]^2\|, \quad (1)$$

where f is a forward operator, d is the measurement data vector, α is a regularization parameter, and W_m is a model weighting matrix related to a reference model m_{ref} (Binley and Kemna, 2005).

Reliable quantification of measurement errors is needed to appropriately condition the inversion (LaBrecque et al., 1996), and the inverse problem needs to be weighted by the measurement error to generate a model with a structure justified by the collected data and calculated noise levels (Binley and Kemna, 2005). A widely used method for quantification of measurement error is the reciprocal measurement, whereby the potential and current electrodes are switched. As per the principle of reciprocity, differences between normal and reciprocal errors quantify the error in a measurement (Slater et al., 2000; Koestel et al., 2008).

Resolution of ERI is a complex function of survey design (number of electrodes, electrode spacing, number of measurements, arrangement of electrodes, etc.) and the unknown subsurface resistivity distribution. As the depth of investigation (DOI) increases, the resolution will begin to decrease, due to the decrease in current density in the subsurface. Resolution decreases toward the end of a 2D ERI line because fewer electrodes are available at either side of a survey point. A useful metric for assessing resolution is the DOI index, which quantifies the depth in which the surface electric resistivity survey

becomes insensitive to changes in a reference model (Oldenburg and Li, 1999).

A 48-electrode surface array was oriented perpendicular to the shoreline over the interpreted DH-impacted layer determined from initial site investigation (trenching/coring). This array was 23.5-m long and used 48 stainless steel electrodes at 0.5-m spacing (Figure 3a). The survey used was a custom configuration that combined near-offset dipole-dipole, Wenner, and partially nested arrays de-



Figure 2. Map of the field site showing the locations of the microbiologic samples as well as the location of the resistivity line. Also included are the results of geochemical tests showing the presence of oil (Environmental Response Management Application, 2013).

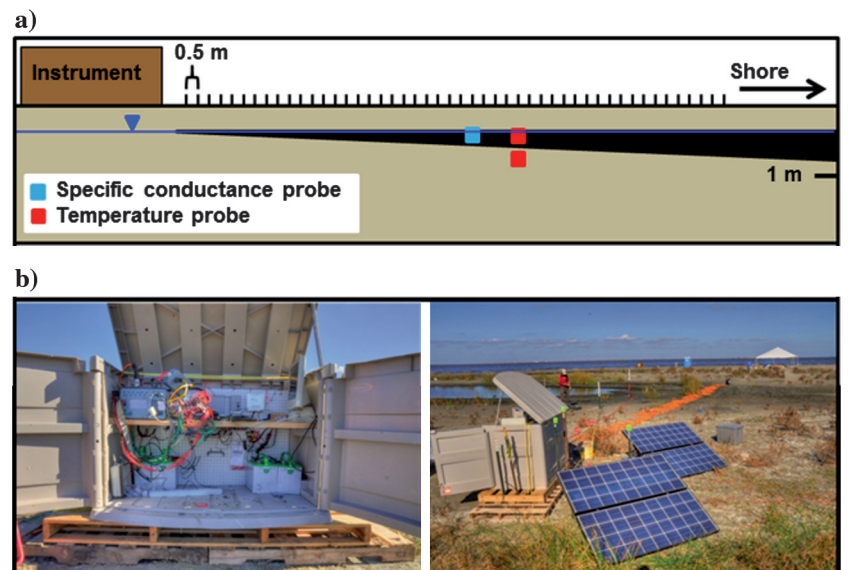


Figure 3. (a) Schematic representation of the field instrumentation. Also included is a projection of the zone of DH contamination interpolated from physical observations in trial pits and projected through the subsurface. (b) The equipment (right) used on the site was solar powered, and the resistivity line (demarcated by the orange resistivity cables on left image) is orientated perpendicular to the shoreline.

signed to provide a large signal-to-noise ratio and minimize data errors. Based on synthetic modeling tests done prior to the survey, this configuration provided comparable resolution to other arrays. The instrumentation was solar powered, the solar panels being used to charge four deep-cycle marine batteries connected to the survey equipment. These batteries, a computer, and a 96-channel IRIS Syscal Pro Resistivity/IP system were encased in a rugged plastic housing to protect them from the elements during normal conditions (Figure 3b).

Measurements were collected twice per day, at 8:00 am/pm. In total, 473 data sets, in addition to reciprocal data sets for error assessment, were collected over approximately 18 months of operation in essentially three measurement periods. The first was from January 2011 to May 2011, the second was from August 2011 to October 2011, and the third was from March 2012 to May 2012. The first data set, collected on 13 January 2011, represented a background data set that was used as a baseline for all of the comparative analyses conducted.

In parallel with the geophysical monitoring, we continuously recorded subsurface temperature and, in the second and third time periods, the specific conductance of the pore fluid, both of which exert a strong influence on resistivity. Temperature loggers were installed with one probe placed in the DH-impacted layer (0.6-m below surface) and the second probe below, in the non-DH-impacted sediment (1-m below surface). A salinity logger directly recorded fluid-specific conductance; this probe was again installed 0.6-m below surface in

the DH-impacted layer. All loggers were installed in slotted PVC pipes providing contact with the fluid in the subsurface.

Error analysis

Assessing measurement error is important to accurately processing and interpreting the data. Reciprocal error analysis is an effective method of calculating these errors (Binley and Kemna, 2005; Koestel et al., 2008). The reciprocal error for each measurement was calculated using

$$\varepsilon_R = \left| \left(\frac{N - R}{N} \right) \right| \times 100, \quad (2)$$

where N is the normal measurement and R is the reciprocal measurement. Any data point with reciprocal error greater than 5% was discarded. If a data set did not meet this criteria for >90% of the data points in that data set, the data set was discarded. In total, 428 of 478 data sets were retained (245/251 for period 1, 109/111 for period 2, and 74/111 for period 3).

It is necessary to assign weights to represent the uncertainties of each measurement in the inversion. Common practice is to use the reciprocal errors of the measured data to develop error models for the input measurements. We followed the approach of Koestel et al. (2008) to describe the absolute reciprocal error as a function of resistance. As a result of the data being collected in three discrete time

periods, three error models were created (Figure 4). All data in each time period were combined and split into 20 equal-size bins based on ascending resistance order. A power law relationship between error and resistance was found to describe each time period (Figure 4a–4c) as well as the entire data set (Figure 4d). Power law model parameters for each individual data set were also determined (Figure 5), from which error weights in the inversion were calculated for each data set. The error model parameters a and b were relatively constant over the first two time periods. The third time period showed an increase in the error model parameters due to the larger reciprocal errors. The specific cause of this increase in reciprocal error is unknown, but was likely related to degradation of the infrastructure due to harsh environmental conditions. This included oxidation of the electrodes and other exposed equipment. It is worth noting that contact resistances on site were consistently very low, less than 1 k Ω and are unlikely to be a significant source of error for the experiment.

Ratio inversion

The inversion code R2 (Binley, 2007) was used to calculate the distribution of the subsurface resistivity using smoothness constraints in the regularization and individual error weights from the error models developed previously. To better visualize the temporal changes in the resistivity over the length of the data series, we also compute ratio resistances:

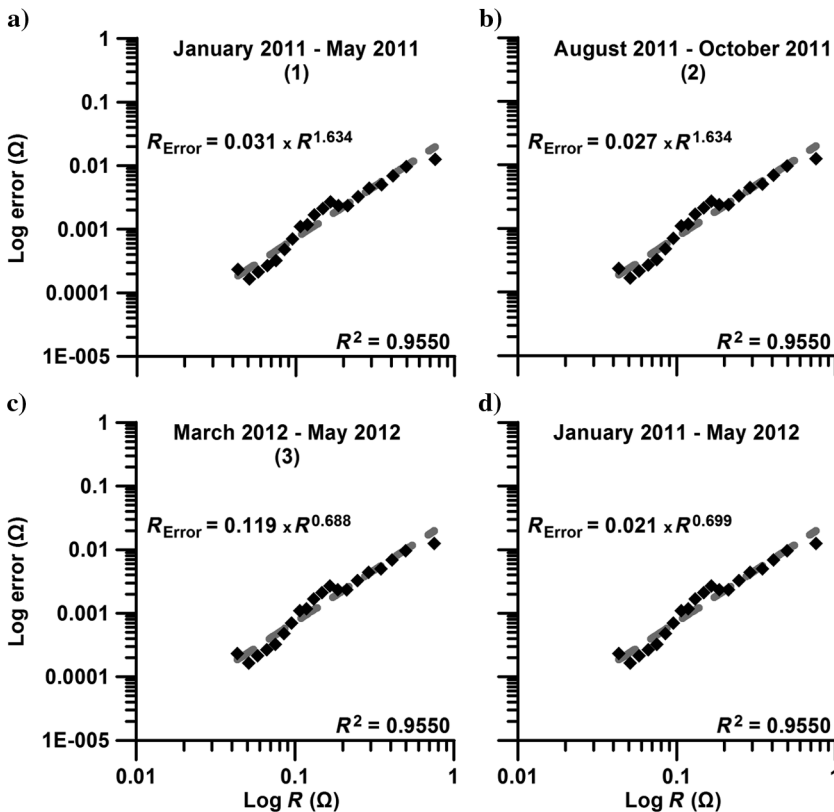


Figure 4. (a–c) Error models from the three distinct collection periods and (d) the error model from the total collection period. The data are represented by the black diamonds, and the equation that fits the data is represented by the gray line. (c) These models distinctly show an increase in measurement error during the March to May 2012 time period.

$$R_{\text{ratio}} = \frac{R_t}{R_0} \times R_f, \quad (3)$$

where R_t is the resistance from the data set of interest, R_0 is the corresponding resistance of the first data set, and R_f is the corresponding resistance of a forward model determined for a subsurface with a homogeneous resistivity distribution (Slater et al., 2000).

When a ratio inversion is used, errors from the two measurements at different times (the measurement at time t , the background measurement at time t_0) and the error associated with the forward model accuracy must be propagated; i.e.,

$$\varepsilon = a\sqrt{(\varepsilon_t)^2 + (\varepsilon_0)^2 + (\varepsilon_F)^2}, \quad (4)$$

where a is a factor increasing the magnitude of the error, ε_t is the error associated with the measurement from the t th data set, ε_0 is the error associated with the measurement from the background data set, and ε_F is the error associated with the forward model. Due to the very low errors in the data, convergence could not be achieved using the weights from the reciprocal error model alone. As a result, the errors were doubled (equation 4) because it allowed for convergence in 2–4 iterations for all of the 428 data sets used, while not overlying smoothing the results.

Temperature correction

Temperature variations in the subsurface affect resistivity measurements, as ion mobility and temperature are directly related (Sen and Goode, 1992). The resistivity will decrease or increase by 2.5% for every 1°C (Keller and Frischknecht, 1966) as the temperature increases and decreases, respectively. These data required a temperature correction because they compared data that spanned the course of more than a year with surveys in each season. Subsurface temperatures measured at the GT1 site varied up to 15°C. The temperature variations in this system were likely driven by solar heating, via conductive and convective heat transfer. On all the inverted images, we normalize the data to 20°C (293°K) using

$$\rho = \rho_T[1 + \beta(T - T_0)], \quad (5)$$

where ρ_T and T are the in situ resistivity and temperature, respectively, T_0 is 20°C (293°K), and β is a temperature coefficient equal to 0.0177 (Shevnin et al., 2007). This was then modified for the ratio resistivity inversion to take the background data set into account using

$$\rho_R = \frac{\rho_0[1 + \beta(T_t - T_0)] - \rho_0}{\rho_0} + \frac{\rho_t}{\rho_0}, \quad (6)$$

where ρ_R is the ratio resistivity, ρ_0 is the corrected resistivity from the background data set, and T_t and T_0 are the temperatures of the data set of interest and background data, respectively. The first term on the right side of the equation represents the correction for the temperature variation alone. This known value, as well as the calculated ρ_R , allows the equation to be solved for the second term on the right. This term is the influence of all the other factors not related to temperature, including variations related to changing subsurface and was the focus of the data interpretation. For this

simplified subsurface temperature distribution, the data from the upper temperature logger were used to correct the resistivity in the upper 0.8 m of the image. Deeper than 0.8 m, the data from the lower temperature logger were used. The temperature correction was applied following the inversion process.

Model resolution

The model resolution, described here by the DOI (Oldenburg and Li, 1999), provides an appraisal of the imaged region in terms of information content and sensitivity to the data acquired. Oldenburg and Li (1999) propose two methods for calculating the DOI for appraisal of model resolution. The method used here compared a single data set regularized to two different homogeneous reference backgrounds. In this method, the DOI index can be calculated by

$$\text{DOI}(x, z) = \frac{m_1(x, z) - m_2(x, z)}{m_{1r} - m_{2r}}, \quad (7)$$

where m_{1r} and m_{2r} are the values used to define the resistivity of the homogeneous background medium of each inversion, and m_1 and m_2 are the results from the inversions. As the DOI index approaches

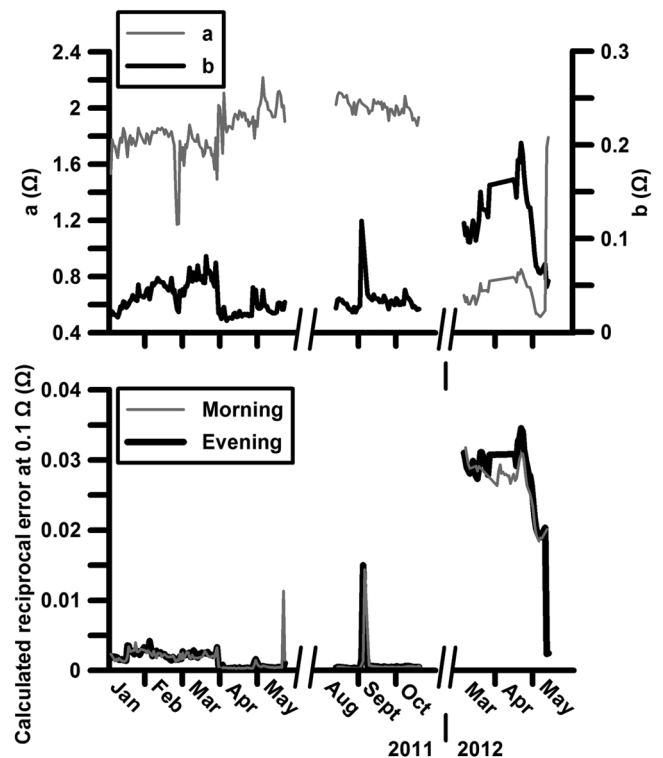


Figure 5. (a) The power law ($e = bxR^a$) error model parameters, a and b , show a relatively constant error model for the first two time periods. The third time period shows a large change in the model parameters due to the larger reciprocal errors. (b) The calculated reciprocal error as a function of time by applying the power law error model to the data. In this case, the error model is calculated individually for each data set. There is a decrease in the measurement error beginning in April 2011 and ending in October 2011. This is related to the deployment of a new, ruggedized cable array. There are two isolated spikes of high measurement error in this time period, although the cause of these is unknown. A significant increase in the error occurred after October 2012.

0, the inversions will produce an identical result for any reference model. As the DOI approaches 1, these values are highly dependent on the reference model and have low credibility (Oldenburg and Li, 1999). The model space is mostly characterized by a DOI below 0.2. The DOI value of 0.2 has been previously determined to be an acceptable degree of resolution (Oldenburg and Li, 1999).

Microbiology

The biodegradation potential of indigenous microbial populations was assessed using microcosms that were set up with sediment samples from DH-impacted as well as nonimpacted areas at the study site (Figure 2). The microbial diversity and microbial community structure of native populations in soil/sediment samples collected from the study site were determined by amplifying 16S rRNA genes using the universal primer sets, 515F and 1391R and the polymerase chain reaction (PCR) method described elsewhere (Sei and Fathepure, 2009). In addition, in situ biodegradation potentials of hydrocarbons at DH-impacted and nonimpacted areas of the study site were determined by screening for the presence of a variety of hydrocarbon-degrading genes that code for monooxygenase and dioxygenase enzymes. Please see the section “Determining microbial diversity and biodegradation potential” in Appendix A for detailed information on determining the diversity and biodegradation potential of the microbes at the site.

RESULTS

Electrical resistivity imaging

It is informative to first analyze the raw measurements before inversion, which introduces complexities from artifacts associated with the regularization constraints. The average resistance of each data set exhibited a general decrease over the duration of the monitoring (Figure 6), the rate being greater at early times, until the end of period 1, when the average resistance decreased by approximately 7% per month. Starting with period 2, the average resistance further decreased, but at a significantly lower rate; during period 3, the average resistance remained almost stable.

Turning next to the inversion results, a resistive feature can be identified in the background image and centered on the DH-im-

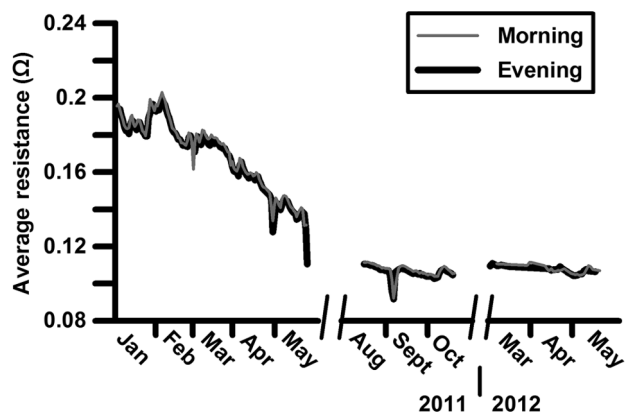


Figure 6. Changes in the average resistance of each data set (700 to 779 measurements) with time. The resistance shows a strong decrease toward the midpoint of data collection of the experiment but then flattens with time.

acted layer at approximately 0.6 m depth (Figure 7), thickening toward the shoreline. Also, this resistive feature overlaid a less-resistive feature, interpreted as being part of the nonimpacted, higher salinity zone below the water table. Between 0 m and approximately 3 m along the line, a resistive anomaly unassociated with the DH oil exists. The inverted images of a small, representative subset of the ratio resistivity inversions illustrate that the resistivity of the interpreted DH-impacted zone decreased with time (Figure 7). The greatest decreases in resistivity seen occurred within the interpreted DH-impacted layer, which showed a consistent decrease in resistivity (ratio resistivity < 1) with time (Figure 7). A near-surface location furthest on the line from the shore (between 0 and 3 m) also showed changes over time. There was no visible contamination at that location on the line, and the larger increases (ratio resistivity > 1) and decreases in resistivity seen here were limited to this region.

Temporal resistivity variations for selected pixels were examined to better illustrate the changes in resistivity within different regions of the image over the entire 473 data sets (Figure 8). Five locations were picked: two in the center of the DH-impacted layer and three outside of this layer, including the varying resistive anomaly. These pixels were considered to be representative of the major features seen in the resistivity data.

The temporal resistivity variations of selected pixels in the DH-impacted layer, denoted by the blue and green lines, show a clear decrease in resistivity with time. The pixel closer to shore (green line) showed a continuous decrease over the duration of the monitoring period, with a greater change over period 1, and a slower decrease over periods 2 and 3. The same behavior was observed for the second location analyzed within the DH-impacted layer, which was further inland (blue line). The points located outside of the DH-impacted layer, denoted by the purple and black lines, showed stable resistivities with time, with a slight increase in some instances. The last point, representative of the area with anomalous behavior (red line), showed proportionally larger changes in resistivity with time.

Specific conductance

The subsurface specific conductance values ranged from 1.1 to 2.5 S/m. The lower specific conductance values occurred in the winter months, and the higher values occurred in the summer months. These data were acquired from the approximate location of the water table, within the DH-impacted sediments. The average value of the specific conductance was 1.73 S/m with a standard deviation of 0.34 S/m, as compared to the average seawater conductivity of 5 S/m (Hanor and Mercer, 2010).

Microbiology

To determine the ability of the native microbial community to degrade hydrocarbons, microcosms with samples from various locations in the DH-impacted regions were constructed, as well as microcosms using the samples collected from a location in the non-DH-impacted area (Figure 2). Figure 9 shows degradation of benzene and toluene in microcosms prepared with soil/sediment samples collected at the center of the resistivity line in the impacted area of the beach (Figure 9a) and from the unimpacted area of the beach (Figure 9b). In addition, the presence of few hydrocarbon-

degrading genes such as 1, 2-CTD, 2,3-CTD, 3,4-PCA, TOD, Phe, Bhp, Nah, and Alk B were tested for in all samples collected at the site. Results show the presence of Phe at all locations including samples collected from the nonimpacted location. Ring-cleaving genes, 1,2-CAT, 2,3-CAT, and 3,4-PCA were detected at the two inland sample locations in the impacted area but not in samples from locations closest to the shore. Ring hydroxylating genes (TOD, Bhp, Nah) and the alkane hydroxylating gene (AlkB) were not detected in any of the tested samples.

The microcosm studies and the survey for the presence of a variety of hydrocarbon degrading genes at contaminated locations are important for understanding the capability of indigenous microorganisms to degrade hydrocarbons. Such information could aid in understanding and advancing bioremediation of contaminated sites. Interestingly, ring hydroxylating gene Phe was detected in all samples including samples from the non-impacted location. Phe is a monooxygenase that catalyzes the initial step in degradation by incorporating a hydroxyl moiety in a variety of aromatic compounds such as benzene, indole, phenol, and substituted phenols (fluoro-, chloro-, amino-, and methyl-phenols) (Neujahr and Gaal, 1973; Neujahr and Kjellen, 1978; Qu et al., 2012) converting these compounds to catechol, which is then broken down by ring cleaving 1,2-CAT and 2,3-CAT and assimilated for growth. Microorganisms with multicomponent phenol hydroxylase are distributed worldwide and seem to be the most ubiquitous in the environment (Sandhu et al., 2009). For further details on the results of the DNA analysis, please refer to the section “Results of DNA analysis” in Appendix A.

DISCUSSION

Resistance data and inverted resistivity images indicate a steady decrease in resistivity of the subsurface for the first five months of data collection, with the largest decreases associated with the DH-impacted zone. The resistance data and resistivity images then begin to stabilize five to six months into data collection, consistent with the conceptual evolution of conductivity shown in Figure 1b as the contaminant matures. These results indicate the viability of resistivity monitoring of the degradation of hydrocarbon contaminants in a remote environment. Our results are consistent with the conductive hydrocarbon degradation model (Atekwana et al., 2000; Sauck, 2000; Bradford, 2007; Cassidy, 2007, 2008; Atekwana and Slater, 2009; Atekwana and Atekwana, 2010), proposing that aging hydrocarbon plumes become less resistive over time. This experiment represents the first field attempt (as far as we are aware) to capture an oil spill from an early stage and study the evolution of the subsurface electric properties as the spill matures. As implied by this conceptual model, the interpreted hydrocarbon contamination at

our site appears to become more conductive over time. Due to the fact that no engineered remediation efforts were performed at the site, and hydrocarbon degrading microbes are in abundance, we infer that the observed decrease in resistivity is likely driven by the microbial degradation of the hydrocarbon contamination.

The single pixel analysis confirmed that the long-term resistivity decreases are strongest in and around the DH-impacted layer (Figure 8). The stabilization of the resistivity between May and August 2011 may potentially signify a decrease in the rate of degradation or the completion of the degradation process. If changes in groundwater composition due to the tide were the driving force on resistivity changes at the site, then resistivity would likely show increases and decreases with time and not the long-term trend to lower resistivity observed here. Furthermore, we would expect that

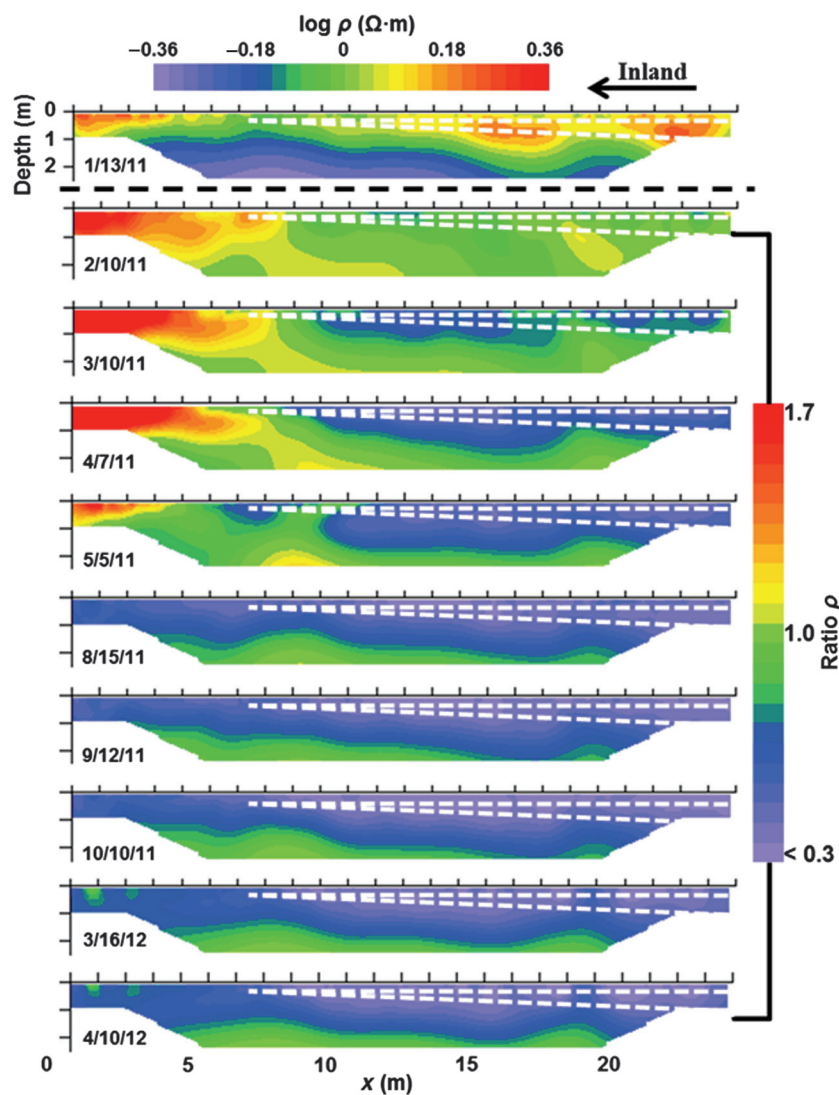


Figure 7. Ratio resistivity images indicate a decrease in resistivity within the DH-impacted layer with time. This layer is located at approximately 0.6–1.0-m depth and is characterized by a higher resistivity anomaly when compared to the surrounding area, with the exception of the inland, shallow resistive anomaly. The location and geometry of this resistivity anomaly is consistent with the inferred location of the DH oil layer in the conceptual model of the site (Figure 3a). In these sections, >1 indicates an increase, 1 indicates no change, and <1 indicates a decrease.

tidal processes would change the conductivity in a similar way inside and outside of the zone of contamination. The distribution of resistivities outside of the DH-impacted layer (Figure 8) indicates that temporal variations in the resistivity were smaller and do not show the trend observed within the DH-impacted zone. The only exception to this was a shallow inland zone in which the changes were not consistent with changes seen in other regions during the experiment. These variations are likely associated with periodic vegetation growth observed at these locations and the resulting variations in moisture content driven by evapotranspiration. Alternatively, these variations may have been driven by gas accumulation resulting from biodegradation processes. This is considered less likely in this specific instance because this region was not located over the contaminated layer.

The increases in pixel conductivity within the contaminated layer coincide with increases in specific conductance seen in this layer as shown in Figure 10, in which the ratio of the first specific conductance measurement to the n th specific conductance measurement is plotted in a time series with the ratio conductivity σ inside (Figure 10) and outside of the contaminated layer (Figure 10). This is consistent with previous studies in which degrading or degraded hydrocarbons were imaged as more conductive anomalies due to degradation by-products such as increased ion concentration in the pore fluid. The ratio conductivity outside of the contaminated layer shows no correlation to the variations in the ratio specific conductance whereas the ratio conductivity within shows the evidence of a positive correlation.

We believe that the low-molecular-weight hydrocarbons, aliphatic as well as aromatic hydrocarbons, are removed through volatilization at the surface. However, this is not a major attenuating

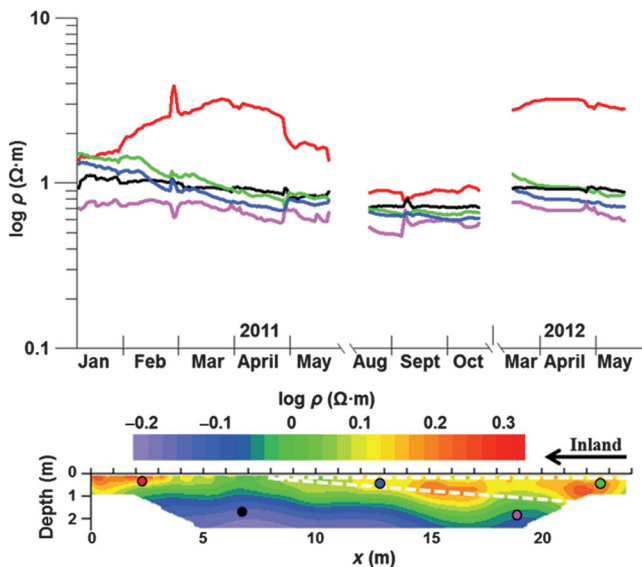


Figure 8. Selected pixel resistivity variation over time. The points within the interpreted DH-impacted zone (green and blue) show a decrease in resistivity over time. The points outside of the DH-impacted zone (black and purple) show much weaker changes in resistivity over the duration of the experiment. The inland and near-surface high-resistivity anomalies (red) show more pronounced fluctuations and larger changes over time. The breaks represent periods in time when the site experienced system outages.

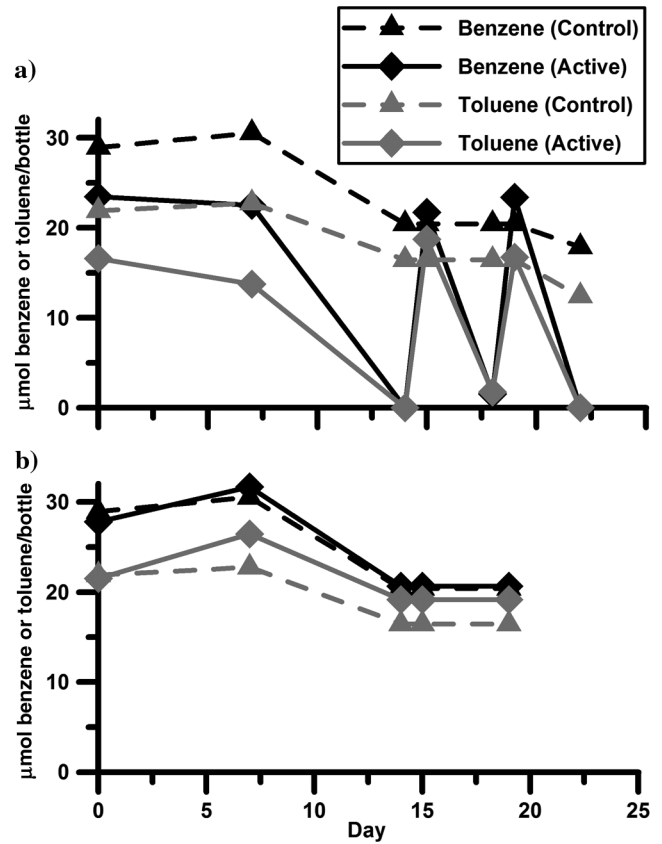


Figure 9. (a) Biodegradation of hydrocarbons in microcosms set up with samples from location 4 (DH-impacted site). Benzene and toluene degraded quickly in active bottles compared to autoclaved bottles suggesting biologic degradation capacity. The secondary spikes in concentration are a result of the active bottles being refed benzene or toluene. (b) Biodegradation of hydrocarbons at location 2 (outside the zone of DH contamination). No appreciable degradation of benzene or toluene occurred in three weeks.

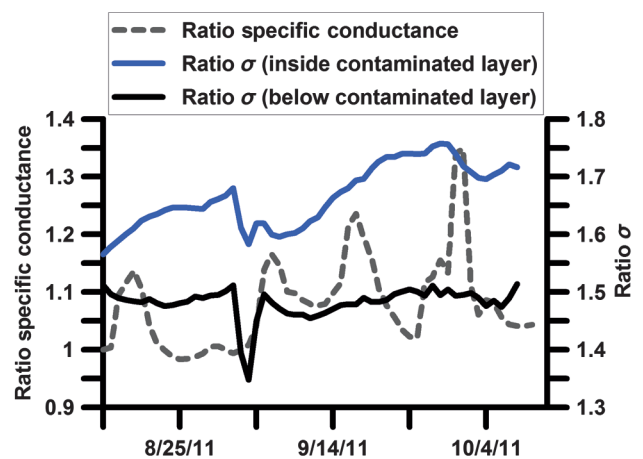


Figure 10. Single pixel ratio conductivities from the second measurement period (inside and outside of the contaminated region, color matched to Figure 8) plotted alongside ratio-specific conductance measurements. The ratio resistivity conductivities from the point outside of the contaminated region remain largely constant. Variations in ratio resistivity from within the contaminated layer are consistent with variations in the ratio specific conductance.

factor in the deeper layers of the sediments. In deeper sections of sediment, biotic processes catalyzed by microorganisms dominate. Microbiological tests confirmed the presence of hydrocarbon degraders in the beach sediments. Different species of hydrocarbon degraders appear to be present throughout the area, and this is expected because Gulf islands and beaches are subjected to hydrocarbon contamination due to small oil spills and natural seeps. Around the monitoring site, in which DH oil was verified to be present, there was less variability in species, with hydrocarbon degraders being the dominant ones. Interestingly, when tested in the laboratory, complete degradation of 17–28 μmol /bottle of benzene and toluene occurred within two weeks for samples from the DH-impacted location (Figure 9a). Furthermore, subsequent addition of the hydrocarbons resulted in increased rates and complete degradation occurring in <7 days suggesting an enrichment of the hydrocarbon-degrading microbial population. On the other hand, negligible amounts of benzene and toluene were degraded in three weeks in microcosms prepared with samples from the location that was not impacted by the DH spill (Figure 9b). This suggested a lack of sufficient microbial activity despite the fact that microbial diversity analysis at this location indicated the presence of organisms with hydrocarbon degradation capacity. The exact reason for the lack of sufficient degradation activity is unknown, but it could be due to a low number of hydrocarbon degraders requiring longer incubations. Alternatively, these organisms may not be adapted for benzene and/or toluene degradation, but for other fractions in crude oil. The rapid degradation of benzene and toluene at the DH-impacted locations suggests that the microorganisms have been recently exposed to hydrocarbons, specifically to the DH spill.

CONCLUSIONS

This experiment demonstrated the viability of long-term ERI monitoring as a technology for noninvasively monitoring the degradation of fresh oil spills in remote coastal environments. The resistivity measurements clearly show a consistent, long-term resistivity decrease within the DH-impacted layer, with limited changes occurring in the surrounding area. Our results suggest that ERI is suitable for deployment in remote areas impacted by hydrocarbon spills. Surface ERI is relatively easy to deploy in comparison with using drilling equipment in areas such as GT1. Our findings suggest that the method might be used to image the oil distribution during early stages of contamination and then monitor the long-term fate of the oil as the degradation progresses.

These results, coupled with the proven abundance of hydrocarbon degraders, lead to the inference that microbial activity within the DH-impacted zone makes a strong contribution to the observed decrease in resistivity. Although this does not provide a strictly quantitative relationship between the stages of degradation of the DH oil, it does provide a qualitative analysis of whether or not the region of DH contamination is undergoing active degradation. The results seen here strongly support the conductive hydrocarbon degradation model because the DH-impacted zone imaged in the survey progressively became more conductive with time.

ACKNOWLEDGMENTS

This work was supported by the United States Environmental Protection Agency National Exposure Research Laboratory, Office

of Research and Development Student Services Contract RFQ-RT-11-00103 to J. Heenan, National Science Foundation RAPID Award, OCE-1049301, American Chemical Society, Petroleum Research Fund, grant no. 49823-ND8, and the Chevron Energy Corporation.

APPENDIX A

DETERMINING MICROBIAL DIVERSITY AND BIODEGRADATION POTENTIAL

Sediment samples, representative of DH-impacted and nonimpacted areas, were collected in sterile plastic containers at various locations and at different depths above the water table at the study site (Figure 2), which, based on physical observation, was collocated with the DH-impacted layer (~60-cm below the surface). The non-DH-impacted area described here refers to a site on GT1 that was not visibly affected by the DH oil spill but is not expected to be “clean” of hydrocarbon contamination. Due to GT1, along with the other barrier islands of the LA coast, periodically receive hydrocarbon contaminants as a result of smaller scale oil spills and naturally occurring oil seeps, it is more accurate if we assume that the impacted area is impacted by the young DH spills, whereas the nonimpacted areas are likely affected by aged hydrocarbons possibly present.

To determine the biodegradation potential of indigenous populations at the site, microcosms were prepared with 160-ml capacity serum bottles containing 10 g of soil/sediment and 40 ml of mineral salts medium (Nicholson and Fathepure, 2004).

Microbial community composition was determined by isolating total DNA from soil/sediment samples using the MoBio ultraclean soil DNA extraction kit (MoBio Laboratories, Carlsbad, California) using the manufacturer’s instructions. 16S rRNA genes were amplified using the universal primer set 515F and 1391R, and PCR method described elsewhere (Sei and Fathepure, 2009).

To determine in situ biodegradation potential of hydrocarbons, we screened for the presence of a variety of genes that code for monooxygenase and dioxygenase enzymes in soil/sediment samples collected at the site. These include catechol 1,2-dioxygenase (1,2-CAT), catechol 2,3-dioxygenase (2,3-CAT), protocatechuate 3,4-dioxygenase (3,4-PCA), toluene dioxygenase (TOD), phenol monooxygenase (Phe), biphenyl dioxygenase (Bhp), naphthalene dioxygenase (Nah), and alkane hydroxylase (Alk B). Total DNA from samples was extracted using the method described above. Ring-hydroxylating and ring-cleaving genes were PCR amplified using above degenerate primers, and the appropriate amplicons were cloned and sequenced to confirm the presence of the hydrocarbon-degrading genes in samples taken at all locations on the site (Baldwin et al., 2003; Sei and Fathepure, 2009; Paisse et al., 2011).

RESULTS OF DNA ANALYSIS

Analysis of 16S rRNA genes revealed the presence of diverse microbial taxa in samples collected from a location on the beach impacted by the BP oil spill (location 4) and what was inferred to be a nonimpacted location (location 2). Analysis showed the presence of a diverse microbial community at both locations regardless of whether hydrocarbons were detected or not in these soil samples. A total of 21–28 bacterial and archaeal taxa were detected. The hydrocarbon-degrading halophilic archaea and bacteria

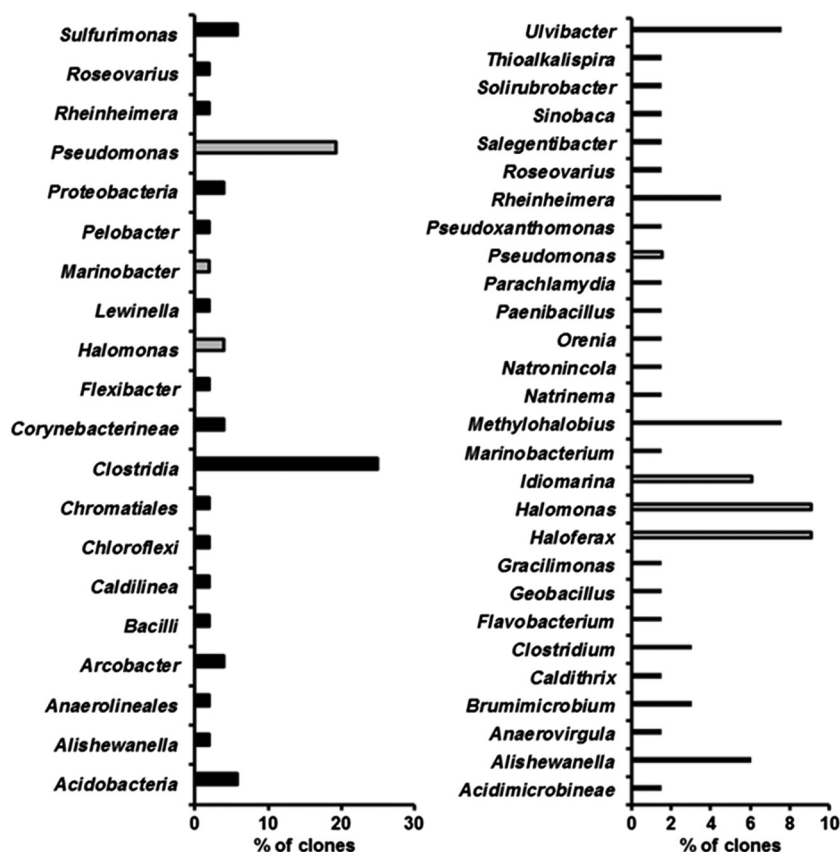


Figure A-1. (a) Microbial community composition at site location 4 (DH oil-impacted location on the beach). *Pseudomonas* sp., *Marinobacter* sp., and *Halomonas* sp. (open bars), are known hydrocarbon degraders. (b) Microbial community composition at location 2 (outside zone of DH contamination). As expected, many hydrocarbon-degrading halophilic organisms are present at this location including *Marinobacter* sp., *Idiomarina* sp., *Halomonas* sp., and an archaeon *Haloferax* sp. (shown as open bars).

such as *Haloferax* sp., *Idiomarina* sp., *Marinobacter* sp., and *Halomonas* sp. were detected at location 2 (non-DH-impacted area). Similarly, hydrocarbon-degrading halophilic bacteria including *Marinobacter* sp. and *Halomonas* spp. were detected at DH-impacted location 4 (Le Borgne et al., 2008). Our analysis showed that phyla *Proteobacteria*, *Bacteroidetes*, *Firmicutes*, *Actinobacteria*, and *Acidobacteria* were found at both locations. Among these, members of *Proteobacteria* and *Firmicutes* were the dominant organisms comprising 25%–30% and 10%–15% of the total clones, respectively. *Halomonas*, *Marinobacteria*, *Idiomarina*, and *Haloferax* were present at both locations, and members of these genera are known as hydrocarbon-degrading organisms in high-salinity environments (Le Borgne et al., 2008) (Figure A-1).

REFERENCES

- Atekwana, E. A., and E. A. Atekwana, 2010, Geophysical signatures of microbial activity at hydrocarbon contaminated sites: A review: *Surveys in Geophysics*, **31**, 247–283, doi: [10.1007/s10712-009-9089-8](https://doi.org/10.1007/s10712-009-9089-8).
- Atekwana, E. A., W. A. Sauck, and D. D. Werkema, 2000, Investigations of geoelectrical signatures at a hydrocarbon contaminated site: *Journal of Applied Geophysics*, **44**, 167–180, doi: [10.1016/S0926-9851\(98\)00033-0](https://doi.org/10.1016/S0926-9851(98)00033-0).
- Atekwana, E. A., and L. D. Slater, 2009, Biogeophysics: A new frontier in earth science research: *Reviews of Geophysics*, **47**, doi: [10.1029/2009RG000285](https://doi.org/10.1029/2009RG000285).
- Atekwana, E. A., D. D. Werkema, and E. A. Atekwana, eds., 2006, *Biogeophysics: The effects of microbial processes on geophysical properties of the shallow subsurface*, in *Applied hydrogeophysics*, Springer, 161–193.
- Baldwin, B. R., C. H. Nakatsu, and L. Nies, 2003, Detection and enumeration of aromatic oxygenase genes by multiplex and real-time PCR: *Applied and Environmental Microbiology*, **69**, 3350–3358, doi: [10.1128/AEM.69.6.3350-3358.2003](https://doi.org/10.1128/AEM.69.6.3350-3358.2003).
- Binley, A., 2007, Freeware — Free resistivity software, <http://www.es.lancs.ac.uk/people/amb/Freeware/R2/R2.htm>, accessed 25 November 2012.
- Binley, A., G. Cassiani, R. Middleton, and P. Winship, 2002, Vadose zone flow model parameterisation using cross-borehole radar and resistivity imaging: *Journal of Hydrology*, **267**, 147–159, doi: [10.1016/S0022-1694\(02\)00146-4](https://doi.org/10.1016/S0022-1694(02)00146-4).
- Binley, A., and A. Kemna, 2005, DC resistivity and induced polarization methods, in *Hydrogeophysics*, Y. Rubin, and S. S. Hubbard, eds., Springer, Water Science and Technology Library, vol. 50, 129–156.
- Bradford, J. H., 2007, Frequency-dependent attenuation analysis of ground-penetrating radar data: *Geophysics*, **72**, no. 3, J7–J16, doi: [10.1190/1.2710183](https://doi.org/10.1190/1.2710183).
- Cassidy, N. J., 2007, Evaluating LNAPL contamination using GPR signal attenuation analysis and dielectric property measurements: Practical implications for hydrological studies: *Journal of Contaminant Hydrology*, **94**, 49–75, doi: [10.1016/j.jconhyd.2007.05.002](https://doi.org/10.1016/j.jconhyd.2007.05.002).
- Cassidy, N. J., 2008, GPR attenuation and scattering in a mature hydrocarbon spill: A modeling study: *Vadose Zone Journal*, **7**, 140–159.
- Crone, T. J., and M. Tolstoy, 2010, Magnitude of the 2010 Gulf of Mexico oil leak: *Science*, **330**, 634, doi: [10.1126/science.1195840](https://doi.org/10.1126/science.1195840).
- Daily, W., A. Ramirez, and A. Binley, 2004, Remote monitoring of leaks in storage tanks using electrical resistance tomography: Application at the Hanford site: *Journal of Environmental and Engineering Geophysics*, **9**, 11–24, doi: [10.4133/JEEG9.1.11](https://doi.org/10.4133/JEEG9.1.11).
- Daily, W., A. Ramirez, D. Labrecque, and J. Nitao, 1992, Electrical-resistivity tomography of vadose water-movement: *Water Resources Research*, **28**, 1429–1442, doi: [10.1029/91WR03087](https://doi.org/10.1029/91WR03087).
- deGroot-Hedlin, C., and S. Constable, 1990, Occam's inversion to generate smooth, two-dimensional models from magnetotelluric data: *Geophysics*, **55**, 1613–1624, doi: [10.1190/1.1442813](https://doi.org/10.1190/1.1442813).
- Ellis, D. E., 2009, Sustainable remediation white paper — Integrating sustainable principles, practices, and metrics into remediation projects: *Remediation*, **19**, 5–114, doi: [11410.1002/rem.20210](https://doi.org/10.1140/1002/rem.20210).
- Environmental Response Management Application, 2013, ERMA deep-water Gulf response, <http://gomex.erma.noaa.gov/erma.html#x=89.37870&y=29.14486&z=6&layers=17770+5723+22869+22881>, accessed 1 April 2013.
- Geospatial Platform Resource Center, 2013, Mapping the response to BP oil spill in the Gulf of Mexico, <http://resources.geoplatform.gov/news/mapping-response-bp-oil-spill-gulf-mexico>, accessed 3 April 2013.
- Hanor, J. S., and J. A. Mercer, 2010, Spatial variations in the salinity of pore waters in northern deep water Gulf of Mexico sediments: Implications for pathways and mechanisms of solute transport: *Geofluids*, **10**, 83–93, doi: [10.1111/j.1468-8123.2009.00271.x](https://doi.org/10.1111/j.1468-8123.2009.00271.x).
- Johnson, T. C., L. D. Slater, D. Ntarlagiannis, F. D. Day-Lewis, and M. El-waseif, 2012, Monitoring groundwater-surface water interaction using time-series and time-frequency analysis of transient three-dimensional electrical resistivity changes: *Water Resources Research*, **48**, W07506, doi: [10.1029/2012WR011893](https://doi.org/10.1029/2012WR011893).
- Keller, G. V., and F. C. Frischknecht, 1966, *Electrical methods in geophysical prospecting*: Pergamon.
- Koestel, J., A. Kemna, M. Javaux, A. Binley, and H. Vereecken, 2008, Quantitative imaging of solute transport in an unsaturated and undisturbed soil monolith with 3D ERT and TDR: *Water Resources Research*, **44**, W12411, doi: [10.1029/2007WR006755](https://doi.org/10.1029/2007WR006755).
- LaBrecque, D., M. Miletto, W. Daily, A. Ramirez, and E. Owen, 1996, The effects of noise on Occam's inversion of resistivity tomography data: *Geophysics*, **61**, 538–548, doi: [10.1190/1.1443980](https://doi.org/10.1190/1.1443980).
- LaBrecque, D. J., G. Heath, R. Sharpe, and R. Versteeg, 2004, Autonomous monitoring of fluid movement using 3-D electrical resistivity tomography:

- Journal of Environmental and Engineering Geophysics, **9**, 167–176, doi: [10.4133/JEEG9.3.167](https://doi.org/10.4133/JEEG9.3.167).
- Le Borgne, S., D. Paniagua, and R. Vazquez-Duhalt, 2008, Biodegradation of organic pollutants by halophilic bacteria and archaea: Journal of Molecular Microbiology and Biotechnology, **15**, 74–92, doi: [10.1159/000121323](https://doi.org/10.1159/000121323).
- Neujahr, H. Y., and A. Gaal, 1973, Phenol hydroxylase from yeast: European Journal of Biochemistry, **35**, 386–400, doi: [10.1111/j.1432-1033.1973.tb02851.x](https://doi.org/10.1111/j.1432-1033.1973.tb02851.x).
- Neujahr, H. Y., and K. G. Kjellen, 1978, Phenol hydroxylase from yeast: Reaction with phenol derivatives: Journal of Biological Chemistry, **253**, 8835–8841.
- Nicholson, C. A., and B. Z. Fathepure, 2004, Biodegradation of benzene by halophilic and halotolerant bacteria under aerobic conditions: Applied and Environmental Microbiology, **70**, 1222–1225, doi: [10.1128/AEM.70.2.1222-1225.2004](https://doi.org/10.1128/AEM.70.2.1222-1225.2004).
- Oldenburg, D. W., and Y. Li, 1999, Estimating depth of investigation in DC resistivity and IP surveys: Geophysics, **64**, 403–416, doi: [10.1190/1.1444545](https://doi.org/10.1190/1.1444545).
- Operational Science Advisory Team, 2011, Summary report for fate and effects of remnant oil in the beach environment, <http://www.restorethegulf.gov/sites/default/files/u316/OSAT2%20report%20no%20-ltr.pdf>, accessed August 15, 2012.
- Paisse, S., R. Duran, F. Coulon, and M. Goni-Urriza, 2011, Are alkane hydroxylase genes (alkB) relevant to assess petroleum bioremediation processes in chronically polluted coastal sediments?: Applied Microbiology and Biotechnology, **92**, 835–844, doi: [10.1007/s00253-011-3381-5](https://doi.org/10.1007/s00253-011-3381-5).
- Qu, Y. Y., S. N. Shi, H. Zhou, Q. Ma, X. L. Li, X. W. Zhang, and J. T. Zhou, 2012, Characterization of a novel phenol hydroxylase in indoles biotransformation from a strain *Arthrobacter* sp. W1: PLoS ONE, **7**, doi: [10.1371/journal.pone.0044313](https://doi.org/10.1371/journal.pone.0044313).
- Robinson, J. L., L. D. Slater, and K. V. Schäfer, 2012, Evidence for spatial variability in hydraulic redistribution within an oak-pine forest from resistivity imaging: Journal of Hydrology, **430**, 69–79, doi: [10.1016/j.jhydrol.2012.02.002](https://doi.org/10.1016/j.jhydrol.2012.02.002).
- Rucker, D. F., J. B. Fink, and M. H. Loke, 2011, Environmental monitoring of leaks using time-lapsed long electrode electrical resistivity: Journal of Applied Geophysics, **74**, 242–254, doi: [10.1016/j.jappgeo.2011.06.005](https://doi.org/10.1016/j.jappgeo.2011.06.005).
- Sandhu, A., L. Halverson, and G. Beattie, 2009, Identification and genetic characterization of phenol-degrading bacteria from leaf microbial communities: Microbial Ecology, **57**, 276–285, doi: [10.1007/s00248-008-9473-9](https://doi.org/10.1007/s00248-008-9473-9).
- Sauck, W. A., 2000, A model for the resistivity structure of LNAPL plumes and their environs in sandy sediments: Journal of Applied Geophysics, **44**, 151–165, doi: [10.1016/S0926-9851\(99\)00021-X](https://doi.org/10.1016/S0926-9851(99)00021-X).
- Sauck, W. A., E. A. Atekwana, and M. S. Nash, 1998, High conductivities associated with an LNAPL plume imaged by integrated geophysical techniques: Journal of Environmental and Engineering Geophysics, **2**, 203–212.
- Sei, A., and B. Fathepure, 2009, Biodegradation of BTEX at high salinity by an enrichment culture from hypersaline sediments of Rozel point at Great Salt Lake: Journal of Applied Microbiology, **107**, 2001–2008, doi: [10.1111/j.1365-2672.2009.04385.x](https://doi.org/10.1111/j.1365-2672.2009.04385.x).
- Sen, P. N., and P. A. Goode, 1992, Influence of temperature on electrical conductivity on shaly sands: Geophysics, **57**, 89–96, doi: [10.1190/1.1443191](https://doi.org/10.1190/1.1443191).
- Shevvin, V., A. Mousatov, A. Ryjov, and O. Delgado-Rodriguez, 2007, Estimation of clay content in soil based on resistivity modelling and laboratory measurements: Geophysical Prospecting, **55**, 265–275, doi: [10.1111/j.1365-2478.2007.00599.x](https://doi.org/10.1111/j.1365-2478.2007.00599.x).
- Slater, L., A. M. Binley, W. Daily, and R. Johnson, 2000, Cross-hole electrical imaging of a controlled saline tracer injection: Journal of Applied Geophysics, **44**, 85–102, doi: [10.1016/S0926-9851\(00\)00002-1](https://doi.org/10.1016/S0926-9851(00)00002-1).
- Slater, L. D., and S. K. Sandberg, 2000, Resistivity and induced polarization monitoring of salt transport under natural hydraulic gradients: Geophysics, **65**, 408–420, doi: [10.1190/1.1444735](https://doi.org/10.1190/1.1444735).
- Versteeg, R., K. Wangerud, A. Richardson, T. Rowe, and G. Heath, 2006, Managing a capped acid rock drainage (ARD) repository using semi-autonomous monitoring and modeling: Presented at 7th International Conference on Acid Rock Drainage.